

***L* dependence of energetic electron precipitation driven by magnetospherically reflecting whistler waves**

J. Bortnik, U. S. Inan, and T. F. Bell

Space, Telecommunications, and Radioscience Laboratory, Electrical Engineering Department, Stanford University, Palo Alto, CA 94305, USA

Received 19 September 2001; revised 16 November 2001; accepted 30 November 2001; published 1 August 2002.

[1] Ray tracing analysis and a first-order treatment of the wave frequency and electron energy dependence of gyroresonant pitch angle scattering reveals the L shell dependence of the time-integrated energetic electron (>150 keV) precipitation flux in the drift loss cone due to a single cloud-to-ground lightning stroke. Primary features of the L dependence are determined by the ray paths of magnetospherically reflecting nonducted whistler waves, as well as the refraction of the wave normal vectors due to ionospheric horizontal electron density gradients at low latitudes. Calculations for lightning source latitudes of 25° , 35° , and 45° , with an assumed “average” ionospheric electron density profile, as well as an International Reference Ionosphere model profile, indicate that horizontal ionospheric electron density gradients can cause the whistler wave energy to focus near the geomagnetic equator on the first magnetospheric traverse, resulting in a spatially narrow precipitation signature at low L shells ($1.4 < L < 1.65$). The magnitude of this low- L peak is found to be sensitively dependent on the local ionospheric density gradients. Subsequent magnetospheric reflections result in a broad precipitation peak at higher L shells ($1.8 < L < 4.2$), which is robustly present, with magnitude being relatively insensitive to lightning source-latitude and ionospheric horizontal gradients. The calculated L dependences were found to be in excellent agreement with drift-loss cone fluxes measured aboard the SAMPEX satellite. *INDEX TERMS:* 2716 Magnetospheric Physics: Energetic particles, precipitating; 7867 Space Plasma Physics: Wave/particle interactions; 2730 Magnetospheric Physics: Magnetosphere—inner; 2772 Magnetospheric Physics: Plasma waves and instabilities; *KEYWORDS:* magnetospherically reflecting, whistler waves, VLF, L dependence, nonducted, precipitation

1. Introduction

[2] This paper is motivated by recent SAMPEX satellite observations of precipitating high-energy (>150 keV) electrons in the drift loss cone (the drift loss cone is differentiated from the bounce loss cone in that mirroring particles do not precipitate within one bounce period but rather within one longitudinal drift period as their mirror altitudes become lower in the vicinity of the South Atlantic Anomaly [Blake *et al.*, 2001]). The drift loss cone fluxes exhibit unique and repeatable L -dependent signatures consistent with those expected from gyroresonant pitch angle scattering induced by nonducted (obliquely propagating) magnetospherically reflecting (MR) whistlers. An example of MR whistlers as detected on the Polar spacecraft is shown in Figure 1. Association of these transient drift loss cone flux enhancements with lightning discharges is also indicated by coincident UARS satellite observations [Blake *et al.*, 2001], which show that the energy spectra of the drift loss cone electrons strongly resemble the energy spectra of lightning-induced electron precipitation (LEP) bursts previously observed in the bounce-loss cone on the SEEP

spacecraft [Voss *et al.*, 1998]. Further indications of the causative role of lightning discharges are provided by global lightning flash occurrence data from the Optical Transient Detector (OTD) instrument on the low altitude (750 km, 70° inclination) OrbView-1 satellite [Christian *et al.*, 1989] which indicates the presence of several large lightning storm centers located westward of the SAMPEX orbit during the observations.

[3] In this paper, we use a ray tracing analysis and a relatively simple treatment of the wave frequency and electron energy dependence of cyclotron resonant pitch angle scattering to estimate the L dependence of drift loss cone LEP enhancements under a variety of ionospheric conditions and source lightning locations. Results obtained serve as a basis for interpretation of the physical origin of drift loss cone enhancements exhibiting a variety of L dependences as observed on low-altitude satellites such as SAMPEX and UARS. The general methodology employed is as follows. On the basis of a cursory review of global lightning data from the OTD instrument, representative locations of low-latitude lightning sources are determined and used in our model calculations. For each different lightning location the electromagnetic radiation from the lightning discharge is determined on the basis of past measurements [Uman, 1984, p. 127], and the propagation

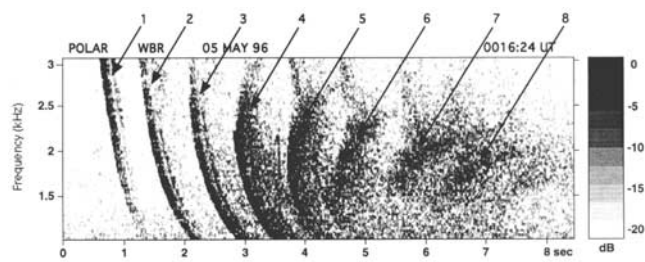


Figure 1. A magnetospherically reflecting whistler train originating from a single lightning discharge observed on the Polar spacecraft. Labels 1–8 indicate the number of “hops” undergone by the whistler.

of this radiation in the Earth-ionosphere waveguide is modeled, allowing for the leakage of a portion of the electromagnetic energy through the ionosphere and into the magnetosphere along the subionospheric propagation path. The lightning frequency spectrum is represented as a superposition of discrete Fourier components. For each wave frequency component the latitudinal spread of the wave energy is in turn represented by tracing a large number of rays.

[4] The injected rays are then propagated numerically through the magnetosphere using the Stanford VLF ray tracing code [e.g., *Inan and Bell, 1977*] to construct a wave property distribution, showing the whistler wave intensity and wave normal vector at each location in the magnetosphere as a function of time. Using this wave property distribution, the relative magnitude of the precipitated energetic electron flux at different L shells is computed and integrated over time to obtain an L -dependent precipitation signature, which can then be directly compared with SAMPEX observations [*Blake et al., 2001*].

[5] Previous studies of wave-induced particle precipitation generally fall into two broad categories. The first category of work deals with quasi steady state representations of the radiation belt particle distribution [e.g., *Kennel and Petschek, 1966*; *Lyons et al. 1971*; *Lyons and Thorne, 1973*; *Abel and Thorne, 1998a, 1998b*] and considers particle lifetimes under wave-driven diffusion but inherently overlooks the causative, transient nature of the events produced by individual discrete wave components. The second category of past work focuses on the transient nature of the wave-particle interaction. For instance, *Inan et al. [1978, 1982]* examined the interaction of parallel propagating, monochromatic whistler waves (ducted whistlers) with energetic electrons using a test-particle formulation; *Chang and Inan [1983, 1985]* extended this analysis to examine coherent waves with slowly varying frequency; *Jasna et al. [1990, 1992]* and *Ristic-Djurovic et al. [1998]* analyzed the interaction of a single pass of a nonducted, monochromatic whistler wave (also considering the steady state case of a whistler wave magnetospherically reflecting back and forth along a single field line), and finally *Lauben et al. [1999]* considered the interaction of a broadband, coherent lightning-generated whistler wave propagating obliquely (nonducted) with energetic electrons but studied only the first pass, as the whistler propagated across the magnetic equatorial into the conjugate hemisphere. In this work we extend past efforts by estimating the time-integrated precipitation

event due to the contributions of both the initial and magnetospherically reflected whistler components, including the full lightning frequency spectrum, using ray tracing to determine the dependence of the precipitation signature on L shell, due to the spatial distribution of the underlying whistler wave energy.

[6] The present work is further differentiated from previous work in that it considers electron flux in the drift loss cone rather than the bounce loss cone. Generally, electrons can be considered stably trapped if the mirror altitude everywhere along their drift orbit is above the dense upper atmosphere (generally taken to be ~ 100 km). If the mirror altitude of an electron at a certain longitude falls below 100 km, it is said to be in the bounce loss cone, since it is lost into the dense atmosphere within approximately one bounce period. However, if the pitch angle of an electron is such that its mirror altitude would fall below 100 km at any longitude along its drift orbit, the particle is said to be in the drift loss cone, recognizing the fact that it would precipitate within one drift period. To illustrate this concept, *Blake et al. [2001]* plot the altitude of the $B = 0.24$ Gauss point as a function of longitude, for $L = 1.6$, showing that an electron that mirrors at this field strength, would always mirror at an altitude >1000 km in the Northern Hemisphere, and typically >1000 km in the Southern Hemisphere, except in the vicinity of $\approx 330^\circ$ longitude, where the South Atlantic Anomaly lowers the mirroring altitude to 100 km. Electrons mirroring at a magnetic field strength >0.24 Gauss are thus trapped within the drift loss cone and are destined to be lost to the dense upper atmosphere within one drift period.

[7] The various important components of our model are described in section 2. The application of the model to a specific case is demonstrated in section 3 where we study the SAMPEX event shown in Figure 4. In section 4, we investigate the variation of the L dependence of the whistler-induced precipitation with different ionospheric and magnetospheric parameters. A mechanism for the formation of narrow peaks at multiple L shells is discussed in section 5, while a summary of major findings, as well as the limitations of the current model are presented in section 6.

2. Description of the Model

[8] The model used here to calculate the L dependence of whistler-induced particle precipitation into the drift loss cone consists of two primary steps. The first step involves the construction of a time-dependent wave property distribution in the magnetosphere, i.e., a specification of the wave properties (electromagnetic power, as well as wave magnetic field intensity B_w , refractive index, and k_{\parallel}) at appropriately discretized spatial points in the magnetosphere as a function of time. For this purpose, ray tracing calculations are performed using a large number of rays, each weighted by a relative power measure, and recorded as a three-dimensional (two spatial and one time) array to be used in the second part of the model calculations. The second step of the model involves the calculation of the contribution to the electron precipitation flux from wave-induced pitch angle scattering occurring at every spatial point in the magnetosphere at each time index in response to the whistler wave launched at $t = 0$, using the wave property distribution developed previously, and subsequently integrating over time to obtain the precip-

itation flux versus L shell signature as would be observed in the drift loss cone.

2.1. Lightning Source

[9] The lightning discharge source is modeled in the same manner as described by *Lauben* [1998] who uses the expression of *Uman* [1984, p. 61], giving the power spectral density at a distance R from the source and angle θ to the local vertical of:

$$S(\omega) = \frac{1}{Z_0} \left(\frac{\mu_0 h_e I_0}{2\pi} \right)^2 \left(\frac{\sin \theta}{R} \right)^2 \frac{\omega^2 (a-b)^2}{(\omega^2 + a^2)(\omega^2 + b^2)},$$

where a , b , and I_0 are model parameters set to 5×10^3 , 1×10^5 and -10.53 kA respectively, to give an electric field amplitude at 100 km of 10 V/m. The cloud height h_e was set at 5 km, and the power spectral density was evaluated at the base of the ionosphere, assumed to be at 100-km altitude, at a frequency $\omega = 2\pi f$.

[10] We note that this lightning model was derived for an unbounded medium and is likely to be increasingly inaccurate when the point of interest is moved farther away and reflections from the ionosphere begin to add in to form the total field. In this work we use the approach of *Inan et al.* [1984], who follows from the work of *Crary* [1961] showing that for a typical summer night model ionosphere, attenuation is 20 dB/1000 km ($1/R^2$) for points within 1500 km from the source and 2 dB/1000 km thereafter. To estimate the fraction of power flowing upward through the ionosphere, an additional factor of $\cos(\theta)$ was multiplied into the above formula [*Lauben*, 1998].

2.2. Propagation Through the Ionosphere

[11] Once the wave power density is computed at the base of the ionosphere, it is then translated to the ionosphere/magnetosphere boundary (taken to be at 1000 km) by attenuating the wave with an appropriate (latitude and frequency dependent) factor taken from *Helliwell* [1965, Figures 3–35], as well as a 3-dB coupling and polarization loss. Theoretically, the radiation pattern of the cloud-to-ground lightning stroke exhibits a null directly above the discharge. However, measurements of VLF transmitter signals (which uses short vertical monopole antennas and should thus also exhibit a similar null) at a few thousand km altitude in the magnetosphere indicate a smooth variation with distance [*Inan et al.*, 1984], possibly due to small-scale irregularities that effectively scatter waves as they pass through the lower ionosphere. For this reason, a simple Gaussian curve is fitted to the resultant pattern at 1000 km, and subsequent rays are weighted according to this spatial power distribution.

[12] Before we inject rays into the magnetosphere at 1000-km altitude, we need to take account of an additional factor that is dealt with in greater detail in section 3, namely the refraction of the ray paths due to horizontal electron density gradients, especially prominent at midlatitudes to low latitudes. Previous ray tracing analyses of oblique-whistler wave propagation [*Edgar*, 1972; *Thorne and Horne*, 1994; *Lauben*, 1998] assumed a horizontally stratified ionosphere, launching rays with vertical wave normals at 1000 km. However, the International Reference Ionosphere (IRI) model at latitudes of interest (approximately -25°)

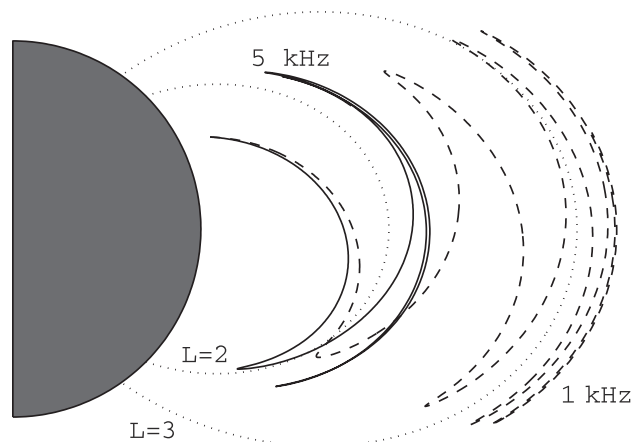


Figure 2. Typical ray tracing paths showing two rays originating at 1000 km, 25° latitude. The 5-kHz ray settles at $L \approx 2.1$, while the 1-kHz ray settles at $L \approx 3$.

predicts strong horizontal gradients at lower altitudes, which tend to refract the nominally vertical wave normals. Ray tracing models of propagation between 100 and 1000 km have revealed that under some conditions, this refraction can be as much as 50° off the local vertical [*James*, 1972].

[13] The refraction of the wave normal vector is very sensitive to the particular ionospheric electron density profile chosen and appears to be a key factor in focusing or defocusing whistler wave energy at specific L shells near the equatorial plane in the magnetosphere [*Sonwalker et al.*, 1995]. This focusing manifests itself as sharp L -dependent peaks in drift loss cone electron precipitation enhancements, as discussed below.

2.3. Propagation Through the Magnetosphere

[14] Whistler wave propagation in the magnetosphere is simulated using the Stanford VLF ray tracing code [*Inan and Bell*, 1977], which is essentially an implementation of a two-dimensional integration of *Haselgrove's* equations [*Haselgrove*, 1954] using a centered dipole model for the magnetic field, and a diffusive equilibrium model [*Angerami and Thomas*, 1964] for the magnetospheric cold plasma. For the purpose of the ray tracing the whistler wave packet is discretized into 21 frequency components spaced approximately logarithmically between 500 Hz and 25 kHz. This level of frequency discretization was chosen since it accurately captured the changes in the precipitation signature as a function of frequency whilst minimizing computation time. The frequency cutoffs were chosen as the -6 dB points of the spectrum relative to its peak. For each frequency, 200 rays are launched, evenly spaced within $\pm 5^\circ$ (in geomagnetic latitude) of the source location. The electron number density is modeled to approximately match typical quiet time magnetospheric conditions, although the precise electron density profile does not affect our results as long as it is smooth as a function of L shell, and there are no sharp plasma density structures (other than the plasma-pause). The reason for this robustness is the fact that the first geomagnetic equatorial crossing of the whistler rays is dominated by the initial wave normal angle of the rays at the entrance to the magnetosphere (1000 km), whereas the settling L shell is determined by the ray frequency being

approximately equal to the equatorial lower hybrid resonance frequency. The exact path followed by each ray from the first equatorial crossing to its settling L shell (which is determined by the electron number density profile) does not significantly affect the final L -dependent precipitation signature. Figure 2 illustrates a typical ray tracing plot of two rays launched at 25° latitude, illustrating how different frequency components separate after the first magnetospheric reflection. In Figure 2, each ray is shown only for the duration of its “effective lifetime,” that is the point at which its power diminishes by 3 dB (due to Landau damping) relative to its initial power.

2.4. Construction of the Wave Property Distribution

[15] In a magnetic meridional plane the magnetospheric space between $0 \leq X \leq 4R_E$ and $-2R_E \leq Y \leq 2R_E$ is discretized into 200×200 bins (where $X = R_{\text{dist}} \cos(\text{latitude})$ and $Y = R_{\text{dist}} \sin(\text{latitude})$ and R_{dist} is the distance measured from the center of the Earth in Earth radii), with 100 time bins making up the third dimension of the data structure. For each frequency, rays are propagated through the magnetospheric grid for the duration of their effective lifetimes (see above), and their instantaneous power density, wave magnetic field intensity B_w , and wave normal vector (i.e., the \mathbf{k} vector) are recorded at every grid point. We note that the wave power density associated with each ray is determined at the entrance to the magnetosphere (1000 km) and then is held constant in accordance with ray tracing theory (allowing only for azimuthal spreading with increasing distance from the Earth). In the case where more than one ray traverses a magnetospheric grid point at the same time bin, it is assumed that the two rays are sufficiently incoherent that their respective powers would be additive and that the square of the total magnetic field intensity at that point and time would be equal to the sum of the squares of that of all the rays that cross that particular spatial bin at that time index. The resultant \mathbf{k} vector was taken to be the vector average of the \mathbf{k} vectors of the different waves at that particular spatial point and time index.

[16] The effects of Landau damping are included crudely as follows. Using the theoretical formulation of *Brinca* [1972] in conjunction with typical suprathermal electron distributions observed by the HYDRA instrument on the Polar spacecraft [Bell et al., 2002] an effective lifetime is calculated for each frequency; that is, the time at which the ray’s power is diminished by 3 dB relative to its initial power. All the rays in the 200 ray group described in section 2.3 are traced with constant power for the duration of the effective lifetime and nulled thereafter.

[17] The resulting wave intensity distribution at selected times is displayed in Figure 3, showing the superposition of the wave power density of all 21 frequency components. Note how the wave packet reflects at high latitudes in the magnetosphere, crossing the magnetic equator multiple times as it slowly moves to higher L shells, resulting in the typical frequency-time signature shown in Figure 1.

2.5. Modeling of the Wave-Induced Precipitation

[18] Using the wave property distribution obtained in section 2.4 (available for only one frequency at a time), the precipitating particle flux at every point and time can,

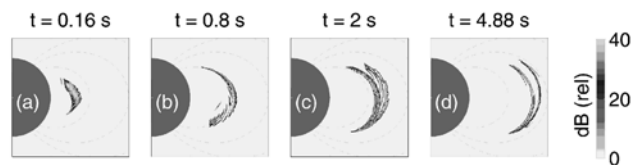


Figure 3. The sequence of parts a–d show the progression of a lightning generated whistler wave power through the magnetosphere at different times. The wave power is magnetospherically reflected in both hemispheres and moves to higher L shells before finally decaying.

in principle, be computed using a test particle approach similar to that used by *Chang and Inan* [1985]. However, this approach is computationally intensive because of the large volume of space occupied by the waves. Our goal is instead to estimate the precipitated flux using a much simpler interaction model that nonetheless clearly brings out the L dependence of the precipitation. As discussed in Appendix A, we expect the precipitation flux at any point to be given by the relation:

$$\Delta \text{flux} \propto \frac{B_w v^2}{v_{\parallel R} E^3 \gamma^4}, \quad (1)$$

where

$$v_{\parallel R} = \frac{\omega_H / \gamma - \omega}{k_{\parallel}} \quad (2)$$

and where Δflux is the electron flux scattered into the loss cone within a particular magnetospheric spatial grid, ω_H and ω are the local gyrofrequency and wave frequency respectively, \mathbf{k} is the wave vector, and B_w is the magnetic field intensity of the wave responsible for changing the pitch angle of the highly energetic electrons under consideration, $\gamma^{-1} = (1 - v^2/c^2)^{1/2}$ is the relativistic Lorentz factor, $v_{\parallel R}$ is the component of the resonant velocity of interacting particles along the static magnetic field, and finally the E is the energy of the resonant electron. Full derivation of equation (1) is given in Appendix A.

[19] The above equation represents a first order approximation designed to bring out the L dependence of the whistler-induced precipitation into the drift loss cone. Sample calculations using equation (1) show interaction lengths and locations very similar to those obtained using a test-particle approach, albeit one performed for only the first hop of the wave [Lauben, 1998]. The use of equation (1) implicitly assumes that only resonant electrons are scattered enough to be precipitated. We consider electrons with energies >150 keV, in order to directly compare with SAMPEX data.

2.6. Evaluation of the Total Drift Loss Cone Precipitation Flux

[20] Our goal is to estimate the total drift loss cone precipitation flux enhancement that would be produced by a given lightning discharge. For this purpose, we evaluate the flux contribution from every spatial grid point in the wave property distribution at all time increments, and integrate over all such contributions along each L shell to determine a total precipitation flux versus L shell for a given

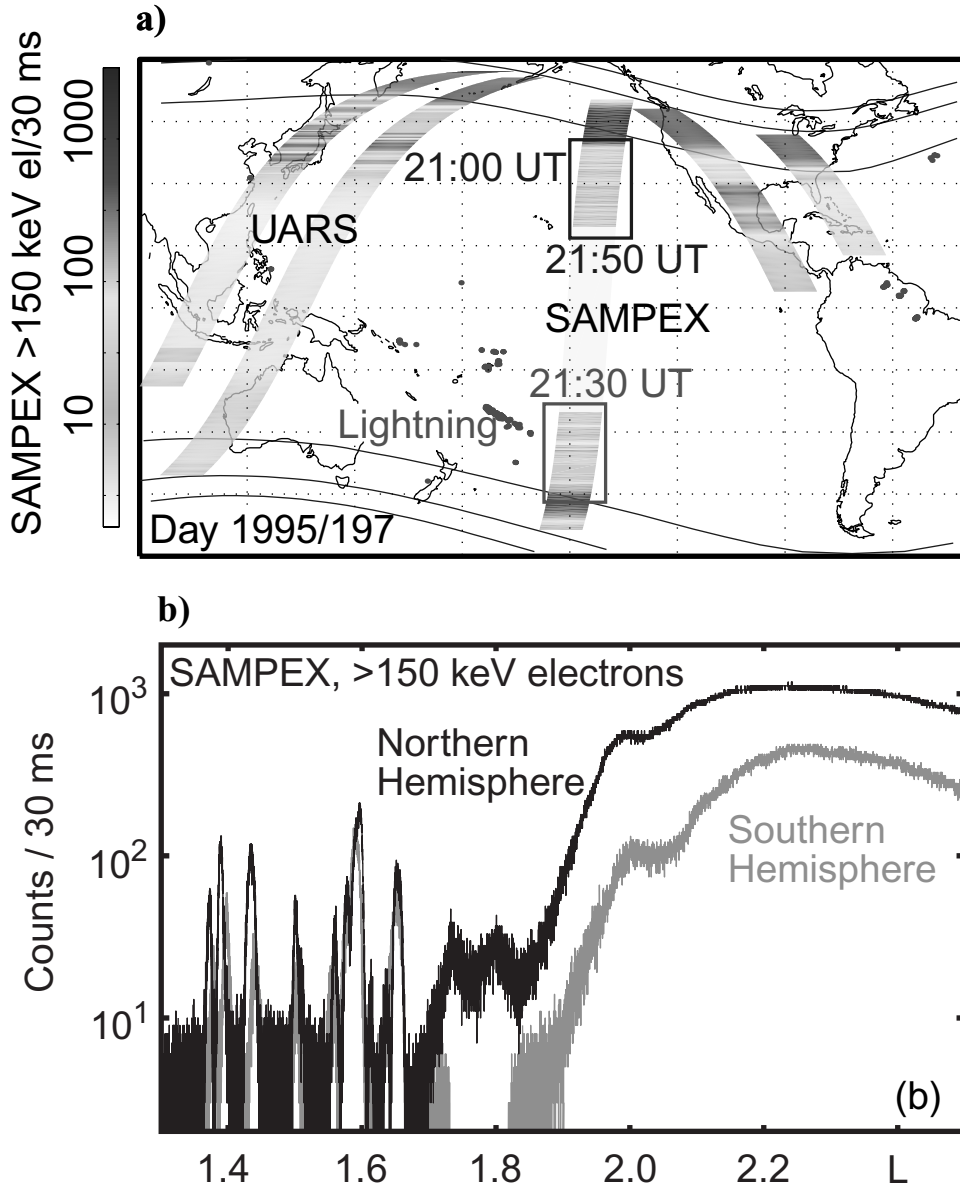


Figure 4. (a) SAMPEX and UARS orbit tracks showing in gray scale the amount of precipitation, and lightning storm locations as recorded on the Optical Transient Detector (OTD) instrument and (b) electron precipitation shown as a function of L shell for above pass on the SAMPEX satellite.

frequency. We then repeat this process for all 21 discrete frequency components.

[21] As a final step, the flux versus L shell values for the 21 frequencies are superposed to obtain a plot of normalized precipitation flux versus L shell, representing the total contributions from all wave components originating at the given lightning discharge. This final integration is implemented by finely interpolating between the different frequency components and summing together the resultant contributions.

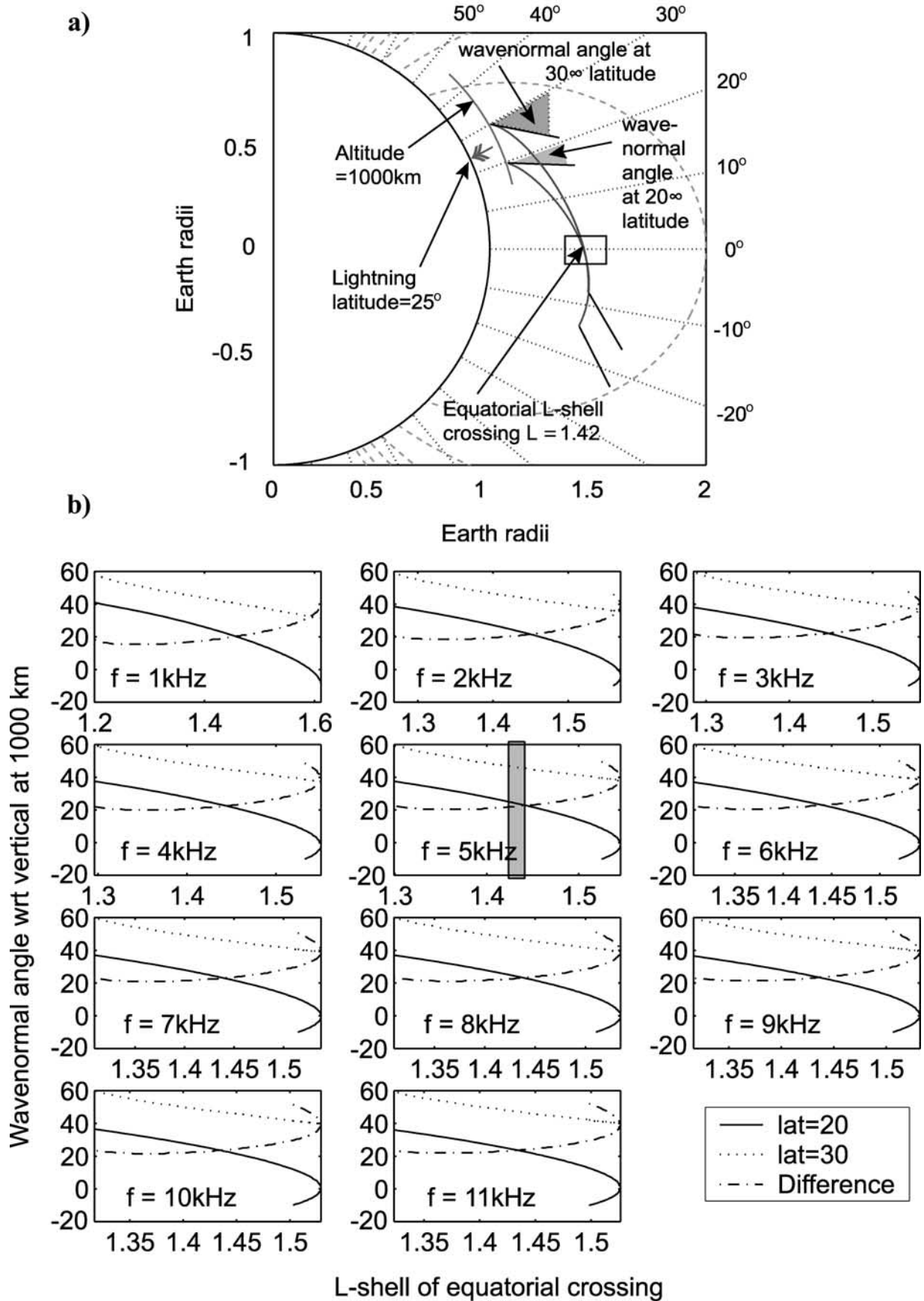
3. Result for Lightning Source Latitude of 25°S

[22] Results for source lightning location at a latitude of 25° (South) is presented as a special case, because of a particularly interesting SAMPEX observation on 16 July 1995 shown in Figure 4 (see also [Blake *et al.*, 2001]). In this

case, relatively rare multiple narrow peaks (in counts/sec) at low L shells ($L \approx 1.4–1.65$) were recorded together with a commonly observed broad precipitation maximum at higher L shells ($L \geq 1.85$). Associated lightning data from the OTD instrument for this case reveals a large thunderstorm center located at $\sim 25^\circ\text{S}$ geomagnetic latitude. In our analysis below we represent this event with a lightning source at 25°N latitude, with the understanding that the dipole field is completely symmetric and that the choice of the Northern Hemisphere as the source location is only for convenience of representation and ease of intercomparison of different cases.

3.1. Convergence of Rays at the Magnetic Equatorial Plane

[23] We launch 200 rays per frequency to simulate the latitudinal spread of the whistler waves, spaced evenly in a



10° latitude range lying between 20° and 30° geomagnetic latitude. On the basis of the relative efficiency of wave-induced pitch angle scattering near the geomagnetic equator, a relatively sharp, low L shell precipitation peak (such as those shown in Figure 4b) would indicate that the whistler energy launched from different latitudinal points may have crossed the magnetic equatorial region in a very narrow spatial region. Such a situation can come about in at least two ways: (1) field-aligned electron density enhancements or depletions (ducts) in the magnetosphere could guide the wave energy, or (2) paths of rays entering the medium at different latitudes may be focused by horizontal density gradients. The first possibility is not likely, owing to relatively rarity of whistler mode ducts at these low latitudes [Cerisier, 1974] and also owing to the fact that the presence of one or more ducts would still not prevent the illumination of the intervening magnetospheric regions with a continuum of nonducted waves, which as shown by *Lauben et al.* [1999] also pitch angle scatter and precipitate electrons. The second possibility is explored in detail below, since horizontal density gradients are very common (see *Kelly* [1989, pp. 192–193] for a discussion of the equatorial anomaly) at low L shells.

[24] To investigate the effects of horizontal density gradients, we analyze the behavior of the two outermost rays (at 20° and 30°) of the ray ensemble in Figure 5, noting that other rays at injection latitudes between 20° and 30° would be bounded by these outer rays. For each L shell shown in the horizontal axis of Figure 5b, the rays with injection latitudes 20° and 30° rays focus on that L shell at the geomagnetic equator, when launched with the wave normal angles (with respect to the local vertical) shown along the vertical axis. For example, the highlighted portion of the 5-kHz plot shows that a 5-kHz ray launched at 20° latitude with a wave normal angle of 24°, and a ray launched at 30° latitude with a wave normal angle of 46° with respect to the local vertical, cross the geomagnetic equator at $L \approx 1.42$. This particular configuration is illustrated schematically in Figure 5a showing the wave normal angles needed at the entry to the magnetosphere (1000 km), and angle differences (dash-dot line), fall within reasonable bounds and in fact, suggest that a single lightning location could easily produce a sharp precipitation peak at a variety of low L shells between $L \sim 1.35$ and $L \sim 1.5$, depending on the particular gradients present in the ionosphere at that time and subsequent resultant configuration of wave normal angles at 1000 km.

3.2. Focusing Due to Horizontal Ionospheric Density Gradients

[25] In order to determine whether reasonable ionospheric density gradients can lead to the refraction of the wave normal vectors in a manner such as to produce equatorial focusing, a particular model ionosphere is constructed using the formulation of *Angerami and Thomas* [1964] with superimposed field aligned density structures according to the formulation of *Bernhardt and Park* [1977].

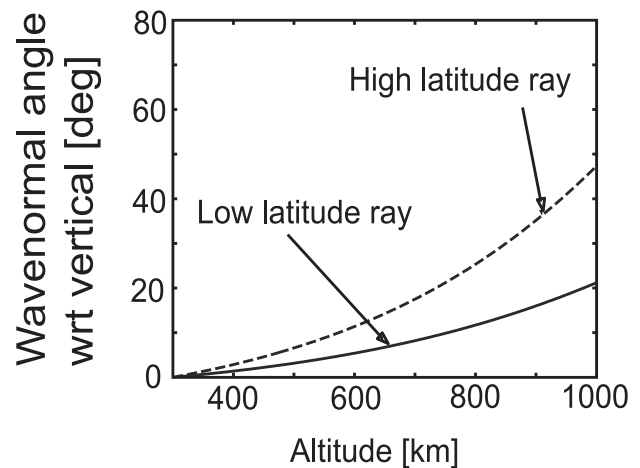


Figure 6. Schematic of the wavenormal angle with respect to the vertical of the rays at -20° and -30° (low-latitude and high-latitude rays respectively), as they traverse the ionosphere from 300- to 1000-km altitude through the model ionosphere shown in Figure 7.

We assume that rays entering the bottomside ionosphere at 100 km become vertical by the time they reach 300-km altitude, due to the sharp boundary at the bottom of the lower ionosphere and the resultant high positive gradient in electron number density. Beyond 300-km altitude, rays are traced through the model ionosphere to determine final topside wave normal angles as shown in Figure 6. Note that the model ionosphere producing such refraction of wave normal vectors is not unique, in that the horizontal gradient at -20° and -30° rather than the absolute density (and magnetic field intensity, dip angle, etc.), is dominantly important in the rotation of the wave normal vectors off the vertical direction [James, 1972].

[26] The particular ionospheric model chosen is illustrated in Figure 7, showing electron number density at 1000-km altitude as a function of latitude. Since rays are traced in two dimensions, the east-west gradient is assumed to be negligible, which is a valid assumption in the midnight sector, where latitudinal gradients dominate longitudinal gradients (International Reference Ionosphere model, see *Bilitza* [1990, and references therein]). This model ionosphere, shown as solid line in Figure 7, is chosen to be representative of different ionospheric gradients observed at these latitudes. A number of latitudinal electron density profiles are plotted (dashed lines) in Figure 7 for comparison, representing profiles obtained for different longitudes on 16 July 1995, 2100 UT (the International Reference Ionosphere model results were obtained from the Web pages of NASA's National Space Science Data Center [Bilitza, 1990]).

3.3. Pitch Angle Scattering and Interpolation

[27] Using the initial injection wave normal angles at 1000 km, we now establish the wave property distribution at

Figure 5. (opposite) (a) Two rays launched at 20° and 30° latitude respectively, focusing on the magnetic equatorial plane. (b) A full analysis of 11 frequencies showing the wavenormal angle required at 20° launch latitude (solid line) and 30° launch latitude (dotted line) for the rays to focus on the abscissa crossing, e.g., the shaded rectangle illustrates the numbers used in Figure 5a above, showing that when $\psi(\text{latitude} = 20^\circ) = 24^\circ$ and $\psi(\text{latitude} = 30^\circ) = 46^\circ$, focusing takes place at $L \approx 1.42$.

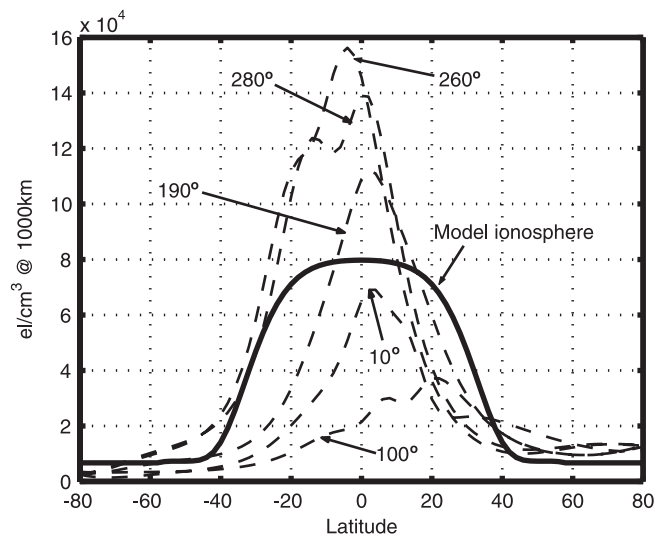


Figure 7. Assumed ionospheric electron number density used in ray tracing model, plotted together with International Reference Ionosphere (IRI) model ionospheres for 16 July 1995 (same day as the SAMPEX pass shown in Figure 4) at various longitudes at 2100 UT.

each frequency and compute the particle precipitation due to each of the frequency components. Note that after several magnetospheric reflections, different frequency components tend to settle on specific L shells [Draganov *et al.*, 1992], lower frequencies on higher L shells, and vice versa. Thus precipitation occurring on various L shells exhibits distinct energy spectra, commensurate with the frequencies responsible for the resonant interaction (lower frequencies scattering higher-energy particles and vice versa). For our calculations we confine the wave-particle interaction to $\pm 5^\circ$ around the geomagnetic equator, based on the work of Lauben [1998], who used a full test-particle calculation for the first pass of the whistler waves to show that the longest wave-particle resonance interaction region (and hence the largest amount of resultant pitch angle scattering) was limited to a region of $\sim 10^\circ$ centered around the geomagnetic equator.

[28] This process is repeated for each of the 21 frequency components covering the range from 0.5 to 25 kHz, using interpolation to determine the contributions of intermediate frequency components. Such interpolation is justified since the L dependence of the precipitation varies slowly with frequency. The final integrated and normalized plot of the L -dependent precipitation flux produced by a lightning source at 25° latitude is shown in Figure 8a.

3.4. Discussion

[29] The similarities between the result shown in Figure 8a to the SAMPEX data in Figure 4b, are readily apparent. Figure 8a exhibits a sharp, low L shell precipitation peak at $L \approx 1.42$, and, a broad precipitation peak at higher L shells of $L \approx 1.9$ –4. The shape of the broad precipitation peak in Figure 8a bears a particularly marked resemblance to that in Figure 4b. Note that the relative magnitude of the low L peak, and the higher L shell peak are somewhat different, as we further discuss in section 5. The fact that the SAMPEX

data in Figure 4b exhibits multiple rather than a single narrow L shell peak is discussed in section 4.

4. Effect of Latitudinal Gradients on the Precipitation Signature

[30] Using the methodology outlined in section 3, we now examine the effects of a number of different latitudinal ionospheric electron density profiles on the precipitation signature. Our aim here is to develop a qualitative guideline to predict the conditions under which ray path focusing effects occur due to horizontal ionospheric gradients and to suggest a possible explanation for the multiple low L shell narrow peaks observed in the SAMPEX data in Figure 4b.

4.1. IRI Model at 190° Longitude

[31] To directly compare with Figure 8a, the IRI ionosphere at a longitude of 190° is modeled as shown in Figure 7 and rays were traced from 300 to 1000 km through it, assuming a lightning source latitude of -25° as before. The refraction of the wave normal vectors in this case turned out to be more severe, resulting in 71° and 57° with respect to the local vertical, for ray injection latitudes of -20° and -30° , respectively. This refraction is a direct result of the high electron density gradients near these injection latitudes. Note that the ray injected at the lower latitude (-20°) refracts farther away from the vertical than that injected at the higher latitude (-30°), resulting in a “defocusing” of the wave energy. This result is consistent with the observation that the electron density gradient was larger at the lower injection latitude than that at the higher. Analysis of the underlying ray paths (not shown) indicates that the rays crossing the magnetic equatorial plane are rather diffuse (spread out), and reenter the topside ionosphere after the first hop without any magnetospheric reflections due to their high wave normal angles. The resultant associated integrated precipitation flux signature

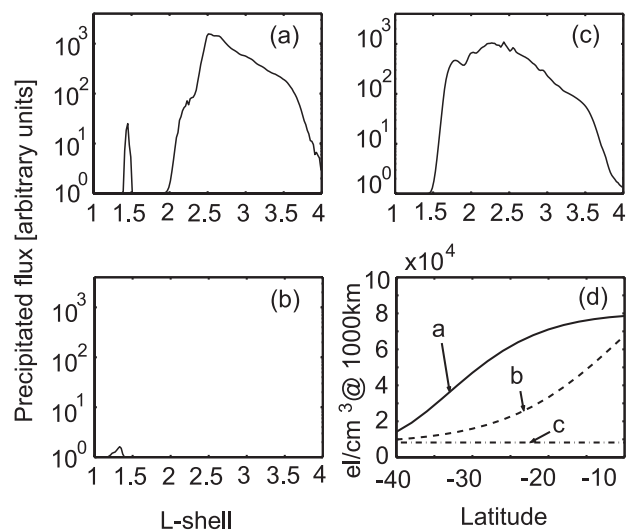


Figure 8. Precipitation flux versus L shell (in arbitrary units) for lightning source latitude is -25° for (a) model ionosphere, (b) IRI model ionosphere at longitude is 190° , 16 July 1995, 2100 UT, (c) horizontally stratified ionosphere. (d) Ionospheric electron density profiles at 1000-km altitude for cases a, b, and c above.

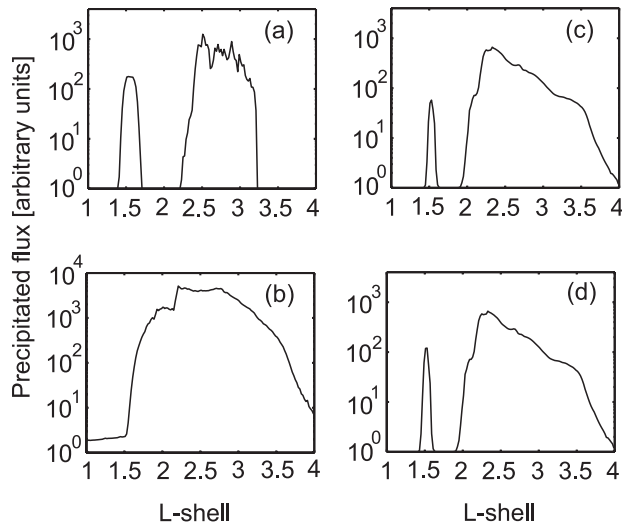


Figure 9. Precipitation flux versus L shell for assumed model density (Figure 7) at (a) lightning source latitude is -35° , (b) lightning source latitude is -45° , note the different vertical scale to previous figures, (c) lightning source latitude is -25° , slightly modified model ionosphere, frequency cutoff is 25 kHz. (d) Identical to Figure 9c except frequency cutoff is 40 kHz.

(Figure 8b) shows a relatively weak low L shell precipitation peak, and no high L shell broad peak, due to a lack of magnetospherically reflected components populating the higher L shells.

4.2. Injection With Vertical k Vectors

[32] The case of injection with vertical wave normal vectors at 1000 km is of particular interest because a strictly horizontally stratified ionosphere is assumed in large body of previous work [Draganov *et al.*, 1992; Edgar, 1972; Lauben, 1998; Lauben *et al.*, 1999; Thorne and Horne, 1994], thus eliminating any possibility of ray focusing or defocusing due to horizontal gradients. The resultant precipitation signature for a lightning source latitude of -25° is shown in Figure 8c and clearly demonstrates the effect of multiple magnetospherically reflected components. Although the broad high L maximum robustly maintains its position, the low L shell peak is in this case spread out and is effectively blended with the broad higher L maximum. This result indicates that a horizontally stratified ionosphere does not lead to low L shell peaks such as those observed in the SAMPEX data.

4.3. Lightning Source Latitude of 35° S

[33] For a lightning source at -35° we trace 200 rays for each frequency for a 10° injection latitude range centered on the source. As can be seen from the model profile of Figure 7, the horizontal latitudinal gradient at -40° is much larger than that at -30° so that the resultant wave normal angles at 1000 km are 76° and 46° , respectively, for rays injected at these two latitudes. The precipitation signature shown in Figure 9a exhibits a somewhat more diffuse low L shell peak, as well as a broad, higher L shell maximum. The presence of the low L peak is manifested by some amount of focusing, although this focusing is not optimal as it is for the

-25° case. Much of the whistler radiation at the higher wave normal angle (76°) is absorbed by the ionosphere, but a fraction is still able to magnetospherically reflect and thus escape to higher L shells, contributing to the formation of the broad peak visible in the range $L \approx 2.2-3.2$.

4.4. Lightning Source Latitude of 45° S

[34] An examination of the model ionosphere of Figure 7 shows that there is a very large horizontal gradient at -40° , causing the wave normal vectors to rotate by 76° off the vertical, but that at -50° , the horizontal gradient is very low, so that the wave normal rotates by only 15° from the vertical. Note that in this case the wave normal vectors refract away from each other, once again resulting in defocusing. Figure 9b shows the resultant precipitation flux versus L shell signature, once again exhibiting the distinct absence of a low L shell precipitation peak, as well as the robust presence of the high L shell, broad precipitation peak at $L \approx 1.5-4.2$. Note also that the precipitation resulting from this lightning source latitude is more intense than that from lower latitudes and that the vertical scale in Figure 9b is appropriately extended.

5. Formation of Multiple Narrow Peaks at Low L Shells

[35] It is clear from Figure 4b that multiple low L shell narrow peaks occur at least some of the time, whereas our model calculations only show one such precipitation peak for a range of focusing conditions. Noting that the drift loss cone flux enhancements observed by SAMPEX represent the sum total of all particles that may have been scattered at longitudes due west of the satellite location, multiple peaks can be attributed to the contributions of a number of different source lightning strokes at different longitudes. Each source lightning can account for one low L shell precipitation peak, but because of the eastward drift of mirroring electrons in the drift loss cone, electrons precipitated by waves originating at different lightning strokes can superpose to form the multiple narrow peak pattern seen in Figure 4b. In this connection we note that the horizontal ionospheric density profiles typically vary with longitude as shown in Figure 7, so that the rays originating at different lightning discharges may focus at slightly different L shells as they cross the geomagnetic equator.

[36] Consider for example, a longitudinal location slightly west of the location of our model ionosphere in Figure 4. Using a slightly modified ionospheric density gradients (as would be the case at a different longitude), a lightning stroke at -25° geomagnetic latitude, would produce wave normal angles at 1000 km of 12° and 42° at injection latitudes of -20° and -30° , respectively. The precipitated flux versus L profile for this case is shown in Figure 9c, where we see that the low L shell peak has now moved to slightly higher L than in Figure 8a, namely to $L \approx 1.5$. We have thus shown that with two slightly different model ionospheres, two distinct peaks can be formed by two different lightning sources. The formation of more peaks is then only a matter of having other lightning strokes occurring at L shells near ionospheric focusing regions.

[37] Another important aspect of the comparison of the result of Figure 8a with the SAMPEX data in Figure 4 is the

fact that the intensity of the low L shell precipitation peak for the latter is a factor of ~ 10 lower than the maximum intensity of the high L peak, whereas that for the former is lower by a factor of ~ 100 , and slightly less in Figure 9c. This discrepancy results from our restriction of the frequency spectrum to frequencies < 25 kHz. The choice of 25 kHz was rather arbitrary, the wave radiated by the lightning discharge at 25 kHz being ~ 6 dB lower in power level than the strongest frequency component at 5 kHz, with 500 Hz being chosen to be the lower-frequency cutoff for the same reason. However, since higher-frequency components resonantly interact with lower-energy electrons, and the available flux of lower-energy electrons is typically much higher than that for higher-energy electrons, the contribution to the precipitation flux of the high-frequency components does not become negligible at 25 kHz in spite of the substantially reduced wave intensity and instead slowly diminish with increasing frequency.

[38] To quantify this effect, Figure 9d shows results for the case when the simulated wave frequency spectrum is extended to 40 kHz. We see that the higher-frequency wave components contribute only to the narrow, low L shell precipitation maximum since their frequency is too high for them to magnetospherically reflect, and thus contribute to the high L shell peak. As a result, the relative magnitude of the low L narrow peak, and high L peak are now about a factor of ~ 5 , comfortably reproducing observed precipitation signatures. We note that since higher-frequency components contribute only to the low L peak, the shape of the wave spectrum radiated by lightning essentially controls the relative magnitudes of the low L , and high L peaks. For example, if the low L and high L peaks are very close together in magnitude, we might then conclude that the source was a relatively rapid lightning discharge producing significant power at high frequencies.

[39] We should mention that in the above model, the trapped electron flux at the loss cone boundary was assumed to be constant with L shell. The trapped flux levels for energetic particles can in fact exhibit substantial variations with L , but this variation is highly dependent on geomagnetic conditions [West *et al.*, 1981] and for simplicity is left out of the formulation. Nevertheless, results for any given variation of trapped flux with L shell can be inferred from those presented here since the precipitated flux is linearly proportional to the trapped flux level at the edge of the loss cone (thus, for a particular precipitation versus L shell signature, e.g., Figure 9c, one simply needs to multiply this curve by the particular trapped flux versus L shell variation).

6. Summary and Conclusions

[40] Our goal in this paper is to quantitatively estimate the L dependence of drift loss cone precipitation induced by obliquely propagating and magnetospherically reflecting nonducted whistlers launched by lightning discharges at inner belt and slot region latitudes. Results presented are compared with a new type of L -dependent precipitation signature observed aboard the SAMPEX satellite. Our model results provide for a quantitative interpretation of the observed features, consisting of low L shell, sharp precipitation peak(s), and a higher L shell, broad precipi-

itation maximum. This particular L dependence is shown to be consistent with that expected from a single lightning stroke, which radiates VLF wave energy into the magnetosphere in the form of nonducted, magnetospherically reflecting whistler mode waves.

[41] The low L shell precipitation peak is attributed to resonant scattering of particles on the first traverse of the geomagnetic equatorial plane by the nonducted whistler. Furthermore, horizontal ionospheric electron density gradients are shown to cause refraction of the whistler wave normal vectors in such a way that the rays can sometimes focus at the magnetic equatorial plane (where the most intense interaction takes place), thus leading to narrow precipitation peaks at low L shells. The high L shell broad precipitation peak is shown to be formed owing to the second and subsequent hops of magnetospherically reflecting whistler waves. The eventual Landau damping of the whistler waves marks the end of the precipitation event caused by a single lightning discharge.

[42] Our results underscore the crucial role that the ionosphere plays in the L dependence of the drift loss cone precipitation. The well-known equatorial ‘‘bulge’’ (or anomaly) [Kelly, 1989, pp. 192–193] in latitudinal ionospheric electron density profiles (Figure 7) focuses or defocuses whistler waves, depending on the location of the lightning strike beneath the ionosphere. While waves from a lightning source at certain locations might be focused by a given horizontal ionospheric density profile, lightning strikes at other locations would tend to get defocused and their contributions would likely not be significant. Thus the presence or the intensity of the low L shell peaks depends on the particular distribution of lightning sources and ionospheric density gradients in effect at any given time.

[43] On the other hand, model calculations for a number of different horizontal ionospheric density gradients confirm the robust presence of the broad high L shell precipitation peak, the existence of which depends primarily on whether rays are able to magnetospherically reflect following their first crossing of the geomagnetic equator, and continue bouncing between hemispheres whilst settling on their own (frequency dependent) preferred L shells. SAMPEX observations are generally consistent with these predictions, indicating that the high L shell broad peak is robustly observed in many cases, while low L shell narrow peaks are relatively rare.

[44] The fact that our calculations and SAMPEX results agree on the presence and robustness of the high L shell precipitation maximum sheds new information on a number of related topics. First, the duration of MR whistlers in the magnetosphere is implied to be far longer than originally estimated by Thorne and Horne [1994], who used particle data from the OGO 3 satellite. Energetic particle fluxes observed with the HYDRA instrument aboard the Polar spacecraft are observed to be consistently lower for the L shells of interest [Bell *et al.*, 2002]. The precipitation flux due to the first crossing of the magnetic equatorial plane by the whistler is typically less than a tenth of the subsequent integrated precipitation flux due to the MR components, and occurs over a comparatively limited range of L shells. On the other hand, the precipitation due to the MR portion of the whistler extends over a much wider range of L shells (e.g., as shown in Figure 8a). Since previous attempts to compute

the lifetime of energetic particles did not consider the effects of MR whistlers [Abel and Thorne, 1998a, 1998b], we believe that inclusion of the MR components will significantly increase the partial contribution of lightning-generated whistlers to the pitch angle diffusion rates and alter the L -dependent equilibrium distribution functions and lifetimes of energetic particles.

6.1. Limitations of the Model

[45] The model that we have chosen to use in the present work has inherent limitations and assumptions that need to be taken into consideration when interpreting the results. First, the method by which precipitating flux due to a whistler wave of a certain frequency is computed, i.e. equation (1), represents a crude approximation to the far more complicated differential equations of motion of the particle under the influence of an oblique wave packet [Bell, 1984], which must be integrated for every particle entering the wave packet, along the geomagnetic field line. While our method does hide some of the microphysics of the interaction, we have found that the shape (i.e., the L dependence) of the time-integrated precipitation signature varies little with the degree of complexity of equation (1) and is to zeroth order, a crude indication of whether whistler wave energy is present or absent at a particular L shell near the magnetic equator.

[46] Equation (1) also assumes that the precipitation is caused predominantly by the first-order gyroresonance interactions, since as shown by Brinca [1972] the higher order gyroresonance interactions are relatively inefficient in scattering electrons in pitch angle. In addition, higher order gyroresonance interactions involve particles of progressively higher energies, which are less abundant. As an example, consider a 5-kHz whistler wave with a wave normal angle of 87.6° at $L = 2$. The first three gyroresonance interactions will take place with electron energies of 196, 604, and 1066 keV respectively, and with a phase space distribution $\propto E^{-3}$ the relative abundances of particles at these energies are 1, 0.03, and 0.006 respectively (normalized to the first gyroresonance abundance). Owing to the relative inefficiency and scarcity of particles involved in higher-order gyroresonance interactions, we consider only first order gyroresonance interactions in our preliminary evaluation of the L -dependent precipitation signatures.

[47] We have accounted for the effects of Landau damping of the whistler waves only so far as to keep each ray at a constant amplitude for the duration of its “lifetime” and turn the amplitude off thereafter. The lifetime is evaluated using the formulation of Brinca [1972] and by tracing the rays until they have diminished in amplitude by 3 dB. While this is only a first-order approximation of the manner by which the wave power density should decrease along its propagation path due to Landau damping, it is nevertheless considered sufficiently accurate for our purposes since it localizes the precipitation due to each whistler ray to the areas where the ray is most intense. Beyond the 3-dB point, the amplitude tends to decay much more rapidly [Thorne and Horne, 1994] so that any subsequent scattering quickly becomes negligible. One obvious area of further work would be to include the

effects of Landau damping more accurately into subsequent models.

Appendix A

[48] We now derive equation (1), which gives the differential contribution to precipitation from a given wave component at a given frequency. For convenience, we repeat equation (1) below.

$$\Delta flux \propto \frac{B_w v^2}{v_{\parallel R} E^3 \gamma^4}. \quad (A1)$$

[49] We begin by considering an empirical fit to an electron distribution function, in the energy range of interest ($E > 150$ keV), specified in E - α space. Distributions of this form have been used previously by Chang and Inan [1983, 1985], with the assumed energy dependence from Inan *et al.* [1985] and Lauben *et al.* [1999] given by

$$f(E, \alpha) = A \frac{1}{E^3} g(\alpha), \quad (A2)$$

where A is a normalizing constant, E is the electron energy, $g(\alpha)$ is a function of the pitch angle α , describing the anisotropy of the particle distribution. In the present work we need to know $g(\alpha)$ only near the drift loss cone, inside of which it is taken to be empty, i.e.,

$$g(\alpha \geq \alpha_{\text{loss cone}}) = 1 \quad (A3)$$

$$g(\alpha < \alpha_{\text{loss cone}}) = 0. \quad (A4)$$

[50] Following an interaction with the wave, the distribution function is perturbed from its initial state. The resonant particles at the edge of the loss cone scatter into the drift loss cone, i.e., those particles whose velocity parallel to the \mathbf{B} field (v_{\parallel}) matches the resonance velocity ($v_{\parallel R}$), i.e.,

$$v = v_{\parallel R} \quad (A5)$$

$$v_{\parallel R} = \frac{\omega_H / \gamma - \omega}{k_{\parallel}}, \quad (A6)$$

where ω_H and ω are the gyrofrequency and the wave frequency respectively, k_{\parallel} is the component of the wave-number (\mathbf{k}) parallel to the \mathbf{B} field, and $\gamma = (1 - v^2/c^2)^{-1/2}$ is the relativistic Lorentz factor. The configuration of resonant particles' pitch angles following the interaction is sinusoidal as a function of initial gyro phase as shown by Inan *et al.* [1978], with half of the initially trapped particles scattering into the drift loss cone (this, of course, implies that the portion of scattered particles precipitated into the drift loss cone is directly proportional to $\Delta\alpha_{\text{max}}$). Although this result was obtained for a linear interaction with parallel propagating whistlers, it can easily be shown that the pitch angle perturbation due to a linear interaction with obliquely propagating waves is also sinusoidal as a function of initial gyro phase, by following a similar methodology as Inan [1977, Appendix A], but using the equations of motion for oblique whistlers as given by Bell [1984, equation (42.a-c)],

or numerically evaluating these equations directly. Considering only the portion of the electron distribution function inside the drift loss cone, we have

$$f_{lc} \propto A \cdot \frac{1}{E^3} \Delta\alpha_{\max}. \quad (\text{A7})$$

[51] Evaluated at $E = E_R$, where E_R is determined from $V_{\parallel R}$ and α_{lc} . Now, expanding the change in pitch angle, $\Delta\alpha$, into a Taylor series and retaining only the first term (under the assumption that $\Delta\alpha$ is small), we get

$$\Delta\alpha_{\max} \approx \frac{\partial\alpha}{\partial t} \Delta t, \quad (\text{A8})$$

where Δt is the interaction time, given approximately as

$$\Delta t \approx \frac{L_i}{V_R} \quad (\text{A9})$$

and L_i is the interaction length, i.e., the distance over which the resonant particle stays in resonance with the wave, given by *Inan* [1987] as

$$L_i = \left[\frac{16\pi \cdot V_R \cdot L^2 \cdot R_E^2}{9\omega_{Heq}} \right]^{1/3} \quad (\text{A10})$$

[52] Typically, $L_i \approx 2000$ km for $L \approx 2$, and it can be shown that this term stays constant within a factor of ≈ 2 in the range of L shells that we are concerned with. We thus treat it as a constant and assert that to first order:

$$\Delta t \approx \frac{1}{V_R}. \quad (\text{A11})$$

[53] According to *Bell* [1984, equation (47)], who derives the differential equations governing the trajectory of a particle that encounters an obliquely propagating, coherent whistler wave with slowly varying amplitude, frequency and wavenumber (assumptions which are very well suited to our present analysis) in the magnetosphere, $\partial\alpha/\partial t$ can be shown to be proportional to the wave's magnetic field amplitude as follows:

$$\frac{\partial\alpha}{\partial t} \propto \frac{B_W}{m\gamma}. \quad (\text{A12})$$

[54] Combining equations (A7), (A8), (A11), and (A12), we obtain a crude model for the behavior of the distribution function in the loss cone:

$$f_{lc} \propto \frac{1}{E^3} \frac{B_W}{m\gamma} \frac{1}{V_R}. \quad (\text{A13})$$

[55] Finally, we convert to a flux value using the relativistic formulation described by *Chang* [1983], which is repeated here for convenience. From conservation of particles the flux Φ is related to the distribution function f using

$$\Phi \cdot dA \cdot d\Omega \cdot dE \cdot dt = f(E, \alpha) \cdot v^2 \cdot dV \cdot d\Omega \cdot v dt \cdot dA. \quad (\text{A14})$$

[56] We can also relate dE and dV as follows:

$$\begin{aligned} dE &= d \left[mc^2 \left(\frac{1}{\sqrt{1-v^2/c^2}} - 1 \right) \right] = \frac{mc^2}{(1-v^2/c^2)^{3/2}} \frac{vdv}{c^2} \\ &= mc^2 \gamma^3 \frac{vdv}{c^2}. \end{aligned} \quad (\text{A15})$$

[57] Combining equations (A14) and (A15), we obtain

$$\Phi = \frac{f(E, \alpha) \cdot v^2}{m\gamma^3}. \quad (\text{A16})$$

[58] Using equation (A16), we can write equation (A13) in terms of flux, as

$$\Delta \text{flux} \propto \frac{B_W \cdot v^2}{E^3 \cdot V_R \cdot \gamma^4} \quad (\text{A17})$$

giving equation (1) as in the text. Note also that all the constants in the expression (such as rest mass, numeric constants, etc.) have been incorporated into the proportionality sign.

[59] **Acknowledgments.** This research was supported by the Airforce Office of Scientific Research under grant F49620-99-1-0339-P00001, as well as by NASA grant NAS5-30371 via subcontract from the University of Iowa. We wish to thank J. Bernard Blake of the Aerospace Corporation, Los Angeles, as well as D. L. Chenette of Lockheed Martin Advanced Technology Center (LMATC), Palo Alto, for supplying the data from the SAMPEX and UARS satellites, respectively.

[60] Janet G. Luhmann thanks the referees for their assistance in evaluating this paper.

References

- Abel, B., and R. M. Thorne, Electron scattering loss in Earth's inner magnetosphere, 1, Dominant physical processes, *J. Geophys. Res.*, 103(A2), 2385–2396, 1998a.
- Abel, B., and R. M. Thorne, Electron scattering loss in Earth's inner magnetosphere, 2, Sensitivity to model parameters, *J. Geophys. Res.*, 103(A2), 2397–2407, 1998b.
- Angerami, J. J., and J. O. Thomas, Studies of planetary atmospheres, 1, The distribution of electrons and ions in the Earth's exosphere, *J. Geophys. Res.*, 69(21), 4537–4560, 1964.
- Bell, T. F., The nonlinear gyroresonance interaction between energetic electrons and coherent VLF waves propagating at an arbitrary angle with respect to the Earth's magnetic field, *J. Geophys. Res.*, 89(A2), 905–918, 1984.
- Bell, T. F., U. S. Inan, and J. Bortnik, The Landau damping of magnetospherically reflected whistlers within the plasmasphere, *Geophys. Res. Lett.*, 10.1029/2002GL014752, in press, 2002.
- Bernhardt, P. A., and C. G. Park, Protonospheric-ionospheric modeling of VLF ducts, *J. Geophys. Res.*, 82(32), 5222–5230, 1977.
- Bilitza, D., (Ed.), International reference ionosphere 1990, *NSSDC 90-22*, Natl. Space Sci. Data Cent., Greenbelt, Md., 1990.
- Blake, J. B., U. S. Inan, M. Walt, T. F. Bell, J. Bortnik, D. L. Chenette, and H. J. Christian, Lightning-induced energetic electron flux enhancements in the drift loss cone, *J. Geophys. Res.*, 106(A2), 29,733–29,744, 2001.
- Brinca, A. L., On the stability of obliquely propagating whistlers, *J. Geophys. Res.*, 77(19), 3495–3507, 1972.
- Cerisier, J. C., Ducted and partly ducted propagation of VLF waves through the magnetosphere, *J. Atmos. Sol. Terr. Phys.*, 36, 1443–1467, 1974.
- Chang, H. C., Cyclotron resonant scattering of energetic electrons by electromagnetic waves in the magnetosphere, *Tech. Rep. E414-1*, Space, Telecommun., and Radioscience Lab., Stanford Univ., Stanford, Calif., Sept. 1983.
- Chang, H. C., and U. S. Inan, Quasi-relativistic electron precipitation due to interactions with coherent VLF waves in the magnetosphere, *J. Geophys. Res.*, 88(A1), 318–328, 1983.
- Chang, H. C., and U. S. Inan, Lightning-induced electron precipitation from the magnetosphere, *J. Geophys. Res.*, 90(A2), 1531–1541, 1985.

- Christian, H. J., R. J. Blakeslee, and S. J. Goodman, The detection of lightning from geostationary orbit, *J. Geophys. Res.*, 94(D11), 13,329–13,337, 1989.
- Crary, J. H., The effect of the Earth-ionosphere waveguide on whistlers, *Tech. Rep. 9*, Radioscience Lab., Stanford Electron. Lab., Stanford Univ., Stanford Calif., 1961.
- Draganov, A. B., U. S. Inan, V. S. Sonwalker, and T. F. Bell, Magneto-spherically reflected whistlers as a source of plasmaspheric hiss, *Geophys. Res. Lett.*, 19(3), 233–236, 1992.
- Edgar, B. C., The structure of the magnetosphere as deduced from magneto-spherically reflected whistlers, *Tech. Rep. 3438-2*, Radioscience Lab., Stanford Electron. Lab., Stanford Univ., Stanford, Calif., March 1972.
- Haselgrove, J., Ray theory and a new method for ray tracing, in *Report of the Physical Society Conference on Physics of the Ionosphere*, pp. 355–364, Cambridge, England, Sept. 1954.
- Helliwell, R. A., *Whistlers and Related Ionospheric Phenomena*, Stanford Univ. Press, Stanford, Calif., 1965.
- Inan, U. S., Non-linear gyroresonant interactions of energetic particles and coherent VLF waves in the magnetosphere, *Tech. Rep. 3414-3*, Stanford Electron. Lab., Stanford Univ., Stanford, Calif., Aug. 1977.
- Inan, U. S., Gyroresonant pitch angle scattering by coherent and incoherent whistler mode waves in the magnetosphere, *J. Geophys. Res.*, 92(A1), 127–142, 1987.
- Inan, U. S., and T. F. Bell, The plasmopause as a VLF waveguide, *J. Geophys. Res.*, 82(19), 2819–2827, 1977.
- Inan, U. S., T. F. Bell, and R. A. Helliwell, Nonlinear pitch angle scattering of energetic electrons by coherent VLF waves in the magnetosphere, *J. Geophys. Res.*, 83(A7), 3235–3253, 1978.
- Inan, U. S., T. F. Bell, and H. C. Chang, Particle precipitation induced by short-duration VLF waves in the magnetosphere, *J. Geophys. Res.*, 87(A8), 6243–6264, 1982.
- Inan, U. S., H. C. Chang, and R. A. Helliwell, Electron precipitation zones around major ground-based VLF signal sources, *J. Geophys. Res.*, 89(A5), 2891–2906, 1984.
- Inan, U. S., D. L. Carpenter, R. A. Helliwell, and J. P. Katsufakis, Subionospheric VLF/LF phase perturbations produced by lightning-whistler induced particle precipitation, *J. Geophys. Res.*, 90(A8), 7457–7469, 1985.
- James, H. G., Refraction of whistler-mode waves by large-scale gradients in the middle latitude ionosphere, *Ann. Geophys.*, 28(2), 301–309, 1972.
- Jasna, D., U. S. Inan, and T. F. Bell, Equatorial gyroresonance between electrons and magnetospherically reflected whistlers, *Geophys. Res. Lett.*, 17(11), 1865–1868, 1990.
- Jasna, D., U. S. Inan, and T. F. Bell, Precipitation of suprathermal (100 eV) electrons by oblique whistler waves, *Geophys. Res. Lett.*, 19(16), 1639–1642, 1992.
- Kelly, M. C., *The Earth's Ionosphere—Plasma Physics and Electrodynamics*, Academic, San Diego, Calif., 1989.
- Kennel, C. F., and H. E. Petschek, Limit on stably trapped particle fluxes, *J. Geophys. Res.*, 71(1), 1–28, 1966.
- Lauben, D., Precipitation of radiation belt electrons by obliquely propagating lightning-generated whistler waves, Ph.D. thesis, Space, Telecommun., and Radioscience Lab., Stanford Univ., Stanford, Calif., Oct. 1998.
- Lauben, D. S., U. S. Inan, and T. F. Bell, Poleward-displaced electron precipitation from lightning-generated oblique whistlers, *Geophys. Res. Lett.*, 26(16), 2633–2636, 1999.
- Lyons, R. L., and R. M. Thorne, Equilibrium structure of radiation belt electrons, *J. Geophys. Res.*, 78(13), 2142–2149, 1973.
- Lyons, R. L., R. M. Thorne, and C. F. Kennel, Electron pitch-angle diffusion driven by oblique whistler-mode turbulence, *J. Plasma Phys.*, 6(3), 589–606, 1971.
- Ristic-Djurovic, J. L., T. F. Bell, and U. S. Inan, Precipitation of radiation belt electrons by magnetospherically reflected whistlers, *J. Geophys. Res.*, 103(A5), 9249–9260, 1998.
- Sonwalker, V. S., U. S. Inan, T. L. Aggson, W. M. Farrell, and R. Pfaff, Focusing of nonducted whistlers by the equatorial anomaly, *J. Geophys. Res.*, 100(A5), 7783–7790, 1995.
- Thorne, R. M., and R. B. Horne, Landau damping of magnetospherically reflected whistlers, *J. Geophys. Res.*, 99(A9), 17249–17258, 1994.
- Uman, M. A., *Lightning*, Dover, Mineola, N. Y., 1984.
- Voss, H. D., M. Walt, W. L. Imhof, J. Mobilia, and U. S. Inan, Satellite observations of lightning-induced electron precipitation, *J. Geophys. Res.*, 103(A6), 11,725–11,744, 1998.
- West, H. I., Jr., R. M. Buck, and G. T. Davidson, The dynamics of energetic electrons in the Earth's outer radiation belt during 1968 as observed by the Lawrence Livermore National Laboratory's spectrometer on OGO 5, *J. Geophys. Res.*, 86(A4), 2111–2142, 1981.

T. F. Bell, J. Bortnik, and U. S. Inan, Space, Telecommunications, and Radioscience Laboratory, Electrical Engineering Department, Stanford University, Palo Alto, CA 94305, USA. (jbortnik@stanford.edu)